



Article

Probing Temperature- and pH-Dependent Binding between Quantum Dots and Bovine Serum Albumin by Fluorescence Correlation Spectroscopy

Zonghua Wang ^{1,*}, Qiyao Zhao ^{1,2,3}, Menghua Cui ^{2,4}, Shichao Pang ⁵, Jingfang Wang ⁶, Ying Liu ^{3,*} and Liming Xie ^{2,4,*}

¹ Laboratory of Fiber Materials and Modern Textile, The Growing Base for State Key Laboratory, College of Chemistry and Chemical Engineering, Shandong Sino-Japanese Center for Collaborative Research of Carbon Nanomaterials, Collaborative Innovation Center for Marine Biomass Fiber Materials and Textiles, Qingdao University, Qingdao 266071, China; zhaoqy@nanocr.cn

² CAS Key Laboratory of Standardization and Measurement for Nanotechnology, CAS Center for Excellence in Nanoscience, National Center for Nanoscience and Technology, Beijing 100190, China; cuimh@nanocr.cn

³ Laboratory for Biological Effects of Nanomaterials and Nanosafety, National Center for Nanoscience and Technology, Beijing 100190, China

⁴ University of Chinese Academy of Sciences, Beijing 100049, China

⁵ School of Life Sciences and Biotechnology, Shanghai Jiao Tong University, Shanghai 200240, China; scpang@sjtu.edu.cn

⁶ Shanghai Center for Systems Biomedicine, Shanghai Jiao Tong University, Shanghai 200240, China; jfwang8113@sjtu.edu.cn

* Correspondence: wangzonghua@qdu.edu.cn (Z.W.); liuy1@nanocr.cn (Y.L.); xielm@nanocr.cn (L.X.); Tel.: +86-532-8595-0873 (Z.W.); +86-186-0020-3627 (L.X.)

Academic Editor: Kevin Critchley

Received: 13 March 2017; Accepted: 21 April 2017; Published: 25 April 2017

Abstract: Luminescent quantum dots (QDs) with unique optical properties have potential applications in bio-imaging. The interaction between QDs and bio-molecules is important to the biological effect of QDs in vivo. In this paper, we have employed fluorescence correlation spectroscopy (FCS) to probe the temperature- and pH-dependent interactions between CdSe QDs with carboxyl (QDs-COOH) and bovine serum albumin (BSA) in buffer solutions. The results have shown that microscopic dissociation constant K'_D is in the range of $(1.5 \pm 0.2) \times 10^{-5}$ to $(8.6 \pm 0.1) \times 10^{-7}$ M, the Hill coefficient n is from 0.4 to 2.3, and the protein corona thickness is from 3.0 to 9.4 nm. Variable-temperature measurements have shown both negative values of ΔH and ΔS for BSA adsorption on QDs-COOH, while pH has a profound effect on the adsorption. Additionally, FCS measurement QDs-COOH and proteins in whole mice serum and plasma samples has also been conducted. Finally, simulation results have shown four favored QD binding sites in BSA.

Keywords: luminescent quantum dots; fluorescence correlation spectroscopy; temperature- and pH-dependent interactions; simulation

1. Introduction

Luminescent quantum dots (QDs) have attracted tremendous interest towards applications in biomedical fields because of their outstanding optical properties, such as extreme brightness [1,2] and tunable emission wavelength, yet with a narrow emission band [3–5]. Meanwhile, toxicity of QDs has been extensively studied at the level of biological macro-molecules [6,7], subcellular organelles [8], cell [9–11], and others [12]. In biological fluids, QDs can be coated by a layer mainly of proteins, as well as other bio-macromolecules [13], which is called a protein corona. The role of the protein corona

masking the designed surface chemistry of QDs is a critical issue because cellular uptake, and its associated physiological response, are regulated by chemical interactions at the nanoparticle surface. The interactions between QDs and serum proteins may impose severe impacts on the function of the proteins and hence cause toxicity [14–16]. Therefore, it is important to examine the interactions between QDs and proteins, which can help understanding the mechanisms of the biological effects of QDs.

Many parameters have important effects on QD-protein interactions, such as size and surface properties of the QDs, the nature of the proteins, the solution medium, the environment (temperature and pH), and so on. Xiao et al. [17] have investigated the binding between CdTe QDs and human serum albumin (HSA) by the fluorescence quenching method, showing that larger size CdTe QDs have higher affinity. Losin et al. [18] have studied temperature effects on the structural and spectroscopic properties of both individual QDs and bovine serum albumin (BSA), and their bio-conjugates, suggesting structural changes of the protein in the conjugates. He et al. [19] have investigated temperature-dependent binding properties of CdTe QDs and revealed that the binding constants decreased with the temperature. Cui et al. [20] have studied the interaction between gold nanoparticles and different serum proteins by dynamic light scattering (DLS), which revealed that surface modification has profound effects on protein coronas. For example, surface modification with long chain polyethylene glycol (PEG) ($M_W = 5$ k) can prevent protein adsorption.

On the other hand, many analytical techniques, such as atomic force microscopy (AFM), gel electrophoresis, DLS, size-exclusion high-performance liquid chromatography (SE-HPLC), circular dichroism spectroscopy (CD), and fluorescence correlation spectroscopy (FCS), have been used to study the interaction between QDs and biomolecules [17–22]. Specifically, FCS is an ultra-sensitive and noninvasive single molecule detection technique based on statistical analysis of the fluctuations of fluorescence emitted from a small, optically well-defined open volume element [23–25]. FCS has the advantage of high-sensitivity, accurate measurement in complex environments, and the ability to evaluate the kinetics and thermodynamic parameters of biomolecule interactions [25–28]. So far, FCS has been widely used to investigate protein conformation [29], DNA hybridization [30], immunoassay [31], single-cell analysis [32], and so on.

In this work, we have investigated temperature- and pH-dependent binding between ZnS/CdSe quantum dots (QDs-COOH) and BSA by FCS in different media, revealing K'_D from $(1.5 \pm 0.2) \times 10^{-5}$ to $(8.6 \pm 0.1) \times 10^{-7}$ M, n from 0.4 to 2.3, protein corona thickness from 3.0 nm to 9.4 nm, and negative ΔH , ΔS , and ΔG . These results showed that the higher temperature weakened the binding of protein to QDs-COOH, while pH had a profound and complex effect. Simulation has been conducted to reveal possible binding sites between QDs and BSA.

2. Materials and Methods

2.1. Materials

Water-soluble carboxyl ZnS/CdSe QDs (QDs-COOH) and ZnS/CdSe QDs capped with PEG (QDs-PEG, M_w of PEG is 2000) were purchased from Wuhan JiaYuan Quantum Dots Co. Ltd (Wuhan, China). BSA ($\geq 98\%$ lyophilized powder, $M_W = 66430$) was purchased from Sigma-Aldrich (St. Louis, MO, USA). Sodium dihydrogen phosphate (NaH_2PO_4) and disodium hydrogen phosphate (Na_2HPO_4) were purchased from Tianjin Hengxing chemical manufacturing company (Tianjin, China). Phosphate buffer with different pH was prepared by mixing NaH_2PO_4 and Na_2HPO_4 (total concentration of 0.2 M). YM-220 ultra-filtration membrane was purchased from USA (Millipore, MA, USA). Serum and plasma were isolated from blood of 6–8-week old mice (CD-1[®](ICR) IGS mice) bought from Beijing Vital River Laboratory Animal Technology Co., Ltd. (Beijing, China). In all experiments, deionized water (>18 M Ω , 0.2 μm membrane-filtered, Millipore, MA, USA) was used.

2.2. Materials Preparation

All of the ZnS/CdSe quantum dots (QDs-COOH and QDs-PEG) were precipitated with 2-propanol to remove free Cd^{2+} and 3-Mercaptopropionic acid (MPA) [33], and then diluted to 8 nM in phosphate buffer with different pH (pH = 6.0, 7.4 and 9.0) and ultrasonicated for 10 min (with the temperature below 348 K) to ensure the full dissolution of QDs, and then purified with the YM-220 ultra-filtration membrane to remove large particles.

BSA protein powder (13.28 g) was dissolved in 2 mL phosphate buffer with different pH (pH = 6.0, 7.4 and 9.0) and then diluted to different concentrations (50 nM to 100 μM). The as-prepared BSA solutions were ultrasonicated for 10 min to ensure the full dissolution of BSA and purified with the YM-220 ultra-filtration membrane to remove large particles. The BSA solutions were freshly prepared for every experiment, or otherwise stored at $-4\text{ }^\circ\text{C}$ to reduce protein aggregation and sedimentation.

Mouse blood was sampled by periorbital puncture [34]. To obtain the plasma, fresh blood was collected in anticoagulant tubes and then centrifuged at room temperature at 3000 rpm for 10 min. The plasma was light yellow in the upper layer of the tube. To obtain the serum, fresh blood was collected in normal tubes without any anticoagulant and kept at room temperature for 2–4 h. Then the blood was centrifuged at room temperature at 3000 rpm for 10 min. The serum could be obtained from the supernatant. All of the blood samples, including plasma and serum, were freshly prepared for every experiment.

2.3. Methods

2.3.1. Physicochemical Characterization of QDs

The morphology and sizes of QDs were imaged by transmission electron microscopy (TEM, Tecnai F20, FEI, Hillsboro, Oregon, OR, USA) at an operation voltage of 200 kV. QD suspension (at a concentration of 8 nM) was dropped onto a copper grid coated by a carbon membrane and then dried at room temperature for TEM imaging. Ultraviolet-visible spectroscopy (UV-VIS) spectra of QDs were acquired on a Lambda 950 spectrophotometer (Perkin-Elmer Corporation, Waltham, MA, USA). The hydrodynamic size and zeta potential of the QDs were measured on a Malvern Zetasizer Nano ZS (Malvern Instruments, Worcestershire, UK).

2.3.2. FCS Measurements

FCS measurements were performed on a home-built system, which was based on an inverted Olympus IX73 microscope. A NKT supercontinuum white-light pulse laser was used as the excitation laser. The repeat frequency, excitation wavelength, and laser power were 3.123 MHz, 592 nm, and 60 μW , respectively. The excitation light was focused by a 60 \times water immersion objective. The fluorescence emitted by the sample was collected by the same objective and detected by an Excelis Detector (SPCM-AQRH-16). Timeharp 200 (PicoQuant, Berlin, Germany) was used for photon-counting. The coverslip used in the cuvette was coated with a layer of PEG (2 k) to avoid adsorption of fluorescent molecule. The temperature was controlled by an mK1000 series temperature controller (INSTEC, Inc., USA).

QD solutions (200 μL , 8 nM) were mixed with the equal volume BSA solutions with different concentrations (50 nM to 100 μM) diluted in different phosphate buffers (pH = 6.0, 7.4, and 9.0). The solution was incubated at different temperatures (298 K, 300 K, 303 K, and 308 K) for 1 h before FCS measurements. Each sample was measured at least three times and then the average was taken to reduce the error.

2.3.3. Data Analysis

FCS curves are fitted by:

$$G(\tau) = \frac{1}{\langle N \rangle} \frac{1}{\left(1 + \left(\frac{\tau}{\tau_i}\right)\right) \left(1 + \omega^2 \left(\frac{\tau}{\tau_i}\right)\right)^{\frac{1}{2}}} \quad (1)$$

For the case of a Gaussian excitation profile, Aragon and Pecora [35] derived the three-dimensional autocorrelation function in terms of the average number of species crossing the focal volume $\langle N \rangle$, τ_i is the residence time of a molecule in the focal volume, and ω is a structure parameter equal to the ratio of the longitudinal to transverse size of the focal volume. The residence time, τ_i , is related to the corresponding diffusion coefficient, D_i , by $D_i = w_{xy}^2 / (4\tau_i)$ for the transverse direction, where w_{xy} represents the radius in the x-y plane direction of the point spread function of the confocal system. The hydrodynamic radius is calculated according to the Stokes-Einstein equation:

$$D_i = k_B T / (6\pi\eta_0 R) \quad (2)$$

where k_B is the Boltzmann constant, T is the absolute temperature, and η_0 is the solvent viscosity, R is the hydrodynamic radius.

To quantify the interactions between BSA and QDs, a model was adopted [36]:

$$d_z([\text{Protein}]) = d_z(0) \sqrt[3]{1 + c \frac{[\text{Protein}]^n}{[\text{Protein}]^n + (K'_D)^n}} \quad (3)$$

where $d_z([\text{Protein}])$ and $d_z(0)$ are the hydrodynamic diameters of QDs with and without protein, respectively, and c is a scaling constant. Since the number of bound protein molecules should be much less than the number of free protein molecules, the total protein concentration was used as free protein concentration. Fitting the dependence of the hydrodynamic radius on protein concentration directly gives the values of the microscopic dissociation constant K'_D and the Hill coefficient n for BSA-QD binding. For positively/negatively cooperative absorption, n is larger/less than 1, respectively. For serum protein adsorption on nanoparticles, n is close to unity [37,38].

2.4. Circular Dichroism (CD) Spectroscopy

CD spectra of QDs-COOH and BSA were recorded at room temperature on a Jasco J-500C spectropolarimeter. The solution of QDs-COOH and BSA was well dispersed in water and buffer with concentration of 0.2 mg/mL in different pH (6.0, 7.4, and 9.0).

2.5. Simulation

The initial structure of BSA was derived from the crystal structure of bovine serum albumin with PDB ID 4F5S (released on 13 May 2012 with 2.47 Å resolution) [39]. The ZnS/CdSe core region in QDs was treated as a spherical structure, and other parts of QDs remain. Both the BSA initial structure and QD models were then parameterized by CHARMM c36m force field parameters [40] and solvated in a rectangular simulation box with explicit TIP3P waters. After salvation, the simulation system was subjected to a steepest descent energy minimization for about 5000 steps, followed by a conjugate gradient for the next 5000 steps and equilibrated by a 500-ps molecular dynamics simulation to reduce the van der Waals conflicts. Finally, 1-ns molecular dynamics simulations were performed using the NAMD package [41] with a temperature of 298 K, periodic boundary, NPT ensembles, and different pH conditions (6.0, 7.4, and 9.0). The SHAKE algorithm was applied to constrain all of the chemical bonds, and atom velocities for start-up runs were obtained based on the Maxwell distribution at 298 K. For our simulation system, 10 independent simulations were carried out with different start-up velocities. The isothermal compressibility was set to 4.5×10^{-5} /bar for the solvent simulations. The electrostatic

interactions were treated by the particle mesh Ewald (PME) algorithm with an interpolation order of 4.0 and a grid spacing of 0.12 nm. The van der Waals interactions were calculated by using a cut-off of 12 Å. All of the molecular dynamics simulations were performed with a time step of 2 fs, and the coordinates for all the simulation systems were saved every 1 ps.

3. Results and Discussion

3.1. Physicochemical Characterization of Carboxyl QDs (QDs-COOH)

The core size of QDs-COOH revealed by TEM (Figure 1a,b) is 4.5 ± 0.5 nm. The hydrodynamic radius of QDs-COOH is 8.5 ± 0.1 nm measured by DLS (Figure 1c). The slightly larger hydrodynamic radius can be due to the electrical double layer on QDs-COOH surfaces. The absorption and emission peaks of QDs-COOH are around 580 and 620 nm, respectively (Figure 1d). The radius size (R) and zeta potential (ζ) of QDs in buffer solutions with different pH are listed in Table 1. All QDs-COOH showed negative surface charge in buffer solutions.

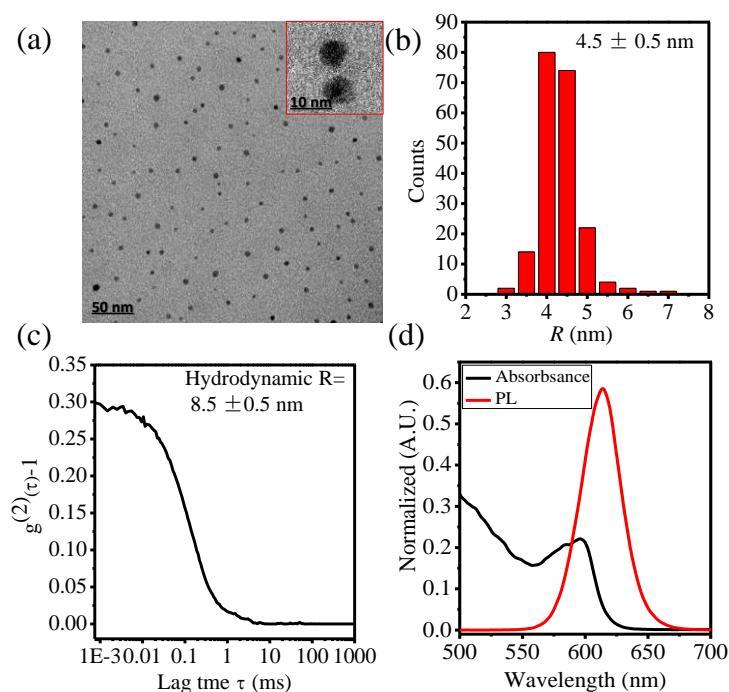


Figure 1. (a) Typical transmission electron microscopy (TEM) image and (b) the corresponding particle size distributions of carboxyl ZnS/CdSe quantum dots (QDs-COOH); (c) Dynamic light scattering (DLS) correlation curves of QDs-COOH; and (d) fluorescence emission spectra and ultraviolet-visible spectroscopy (UV-VIS) spectra of QDs-COOH.

Table 1. List of measured hydrodynamic R and zeta potentials (ζ) of different QDs at different pH (6.0, 7.4, and 9.0).

QDs	pH	R (nm)	Zeta Potential (ζ)
QDs-COOH	6.0	8.6	-7.2
	7.4	8.5	-8.7
	9.0	8.4	-24.0
QDs-PEG	6.0	9.2	-1.9
	7.4	9.4	-6.9
	9.0	9.4	-10.0

3.2. BSA-QD Interaction at Different Temperatures

Typical FCS correlation curves for QDs-COOH with different BSA concentrations (pH = 7.4, T = 298 K) is shown in Figure 2b. The characteristic diffusion time shifts to a longer time at higher BSA concentrations, indicating BSA binding on QDs-COOH. Figure 2c–f show hydrodynamic radii of QDs-COOH derived from the FCS curves at different BSA concentrations and different temperature (300, 303, and 308 K, respectively). Further fitting with Equation (3) give the microscopic dissociation constant K'_D and Hill coefficient n . As the temperature increases, the microscopic dissociation constant (K'_D) gradually increases (weaker interaction) and the protein corona thickness (ΔR) gradually decreases (Figure 2g). Similar results were observed at pH 6.0 and pH 9.0 (Figures S1 and S2). This indicated a decreased affinity between QDs-COOH and BSA at higher temperatures. Further, $\ln K$ is plotted against $1/T$ to extract thermodynamic parameters for BSA-QD interactions according to:

$$\ln K = -\frac{\Delta H}{k_B N_A T} + \frac{\Delta S}{k_B N_A} \quad (4)$$

where K is the binding constant (inverse to K'_D), $k_B N_A$ is the gas constant. The free energy change (ΔG) is then calculated by:

$$\Delta G = \Delta H - T\Delta S \quad (5)$$

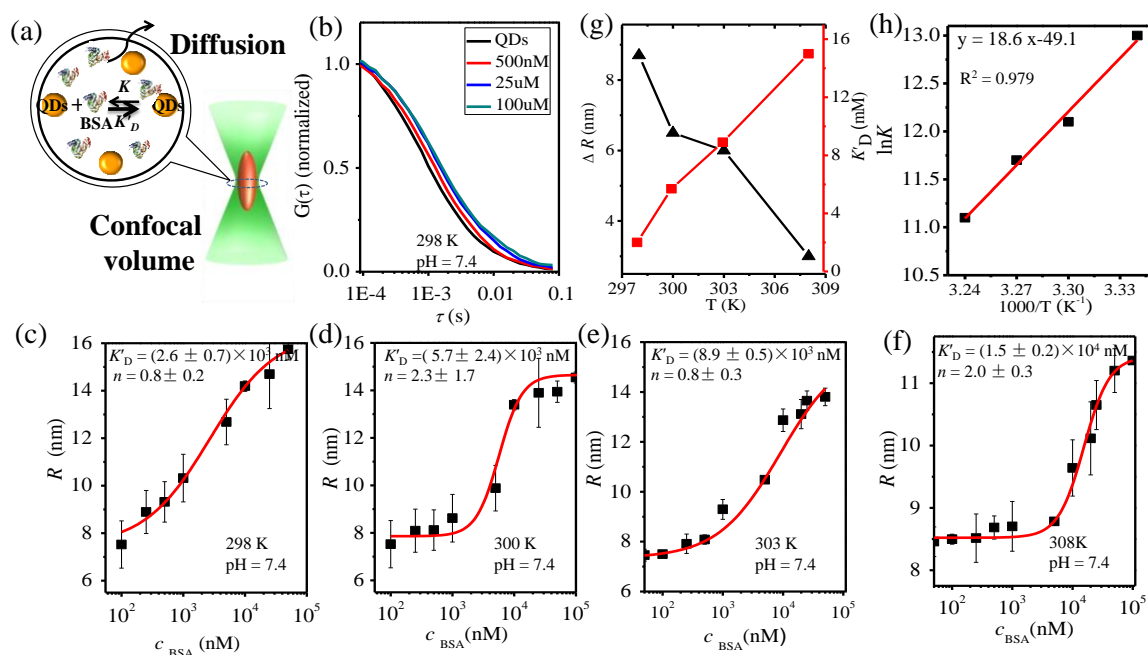


Figure 2. (a) Scheme of FCS system; (b) FCS correlation curves; (c–f) hydrodynamic radii of QDs-COOH at different BSA concentrations (pH = 7.4) at different temperatures (298 K, 300 K, 303 K, and 308 K); (g) Plot of K'_D (red line), ΔR (black line) versus temperature; and (h) the plot of $\ln K$ against $1/T$.

All of the results listed in Table 2 show that $\Delta H < 0$, $\Delta S < 0$, and $\Delta G < 0$. This indicates that the binding of BSA to the QDs-COOH was enthalpy-driven, in which the affinity is lower at higher temperatures. The affinity may be contributed by the hydrogen-bond interactions [42] electrostatic interaction, cavities, or hydrogen-bond interactions [43–46] between QDs-COOH and BSA.

Table 2. Summary of measured K'_D , ΔR , $\ln K$, Hill coefficient n , and ΔH , ΔS , and ΔG for BSA and QDs binding at different pH (6.0, 7.4, and 9.0).

pH	T (K)	K'_D (nM)	n	ΔR (nm)	$\ln K$	ΔH (kJ·mol ⁻¹)	ΔS (J·mol ⁻¹ ·K ⁻¹)	ΔG (kJ·mol ⁻¹)
pH = 6.0	298	$(2.4 \pm 0.4) \times 10^3$	0.4 ± 0.4	8.0	12.9	-1.7×10^2	-4.4×10^2	-33.4
	300	$(4.4 \pm 0.5) \times 10^3$	1.4 ± 0.1	7.5	12.6			-32.7
	303	$(6.6 \pm 3.7) \times 10^3$	0.4 ± 0.1	6.0	11.9			-31.6
	308	$(1.4 \pm 1.3) \times 10^4$	1.0 ± 0.5	5.0	11.2			-29.8
pH = 7.4	298	$(2.6 \pm 0.7) \times 10^3$	0.8 ± 0.2	8.7	12.9	-1.5×10^2	-4.1×10^2	-33.0
	300	$(5.7 \pm 2.6) \times 10^3$	1.3 ± 1.8	6.5	12.3			-32.2
	303	$(8.9 \pm 0.5) \times 10^3$	0.8 ± 0.3	6.2	11.6			-31.0
	308	$(1.5 \pm 0.2) \times 10^4$	1.0 ± 0.3	3.0	11.3			-28.9
pH = 9.0	298	$(8.6 \pm 0.1) \times 10^2$	2.0 ± 0.1	9.4	13.9	-1.1×10^2	-0.7×10^2	-35.1
	300	$(9.5 \pm 3.3) \times 10^2$	2.1 ± 0.3	8.2	13.8			-34.9
	303	$(1.8 \pm 0.4) \times 10^3$	1.6 ± 0.4	7.3	13.7			-34.6
	308	$(2.2 \pm 0.7) \times 10^3$	2.7 ± 0.2	6.7	13.2			-34.0

3.3. BSA-QDs-COOH Interaction at Different pH

Typically, BSA is presented in an N configuration at pH 7.4. But BSA can undergo N-F (normal-fast) transition when $\text{pH} < 5.0$ and N-B (normal-basic) transition when $\text{pH} > 9.0$ [47,48] (Figure 3a). FCS measurements have been done at different pH of 6.0, 7.4, and 9.0 to investigate the interaction of QDs-COOH and BSA (Figure 3b–e). Figure 3c shows the autocorrelation curves for QDs-COOH with BSA at different concentrations at pH 6.0 and Figure 3c–e show hydrodynamic radii at different BSA concentrations at different pH (pH 7.4 and 9.0). K'_D is larger at pH 7.4 than that at pH 6.0 and 9.0 (Figure 3f), indicating a weaker interaction at pH 7.4 and an overall thinner protein corona at pH 7.4 (Figure 3g).

The isoelectric point (i.e., pI) of BSA is 4.7 and $\text{p}K_a$ for carboxyl (-COOH) group is around 5.5 [49,50]. Both BSA and QD-COOH will have more negative surface potentials at higher pH, so weaker interaction is observed at pH 7.4 than that for pH 6.0, which is expected because of the increased repulsion from the more negative charge at the higher pH for both QDs-COOH and BSA. However, stronger interaction is observed at pH 9.0 than that at pH 7.4. BSA might undergo a conformational change [43–45] after combining with QDs-COOH or part of the N conformation of BSA shifts to the basic (B) conformation spontaneously at pH 9.0, and then the secondary and tertiary structures of BSA may change.

The peptide chains of the BSA protein are made up of units, such as α -helicity, β -sheet, and random curliness [51]. Contrasting to the N conformation, the B conformation is characterized by a significant loss in helical content and a phase of a decrease in the secondary structure [52], which results in partial unfolding of the secondary structure. Thus, BSA turns to be a loosening of the molecule with a loss of rigidity [53–55]. In addition, the disruption of tertiary contacts of BSA may be beneficial to the hydrogen bonding reaction between BSA and QDs-COOH. Thus, the more flexible structure of BSA at pH 9.0 can have higher affinity to QDs-COOH.

CD spectroscopy has also been conducted to investigate the secondary structure of BSA before and after binding to QDs-COOH (Figure 4). First, significant loss of the helical structure is clearly seen for BSA at pH 9.0 (Figure 4a). In the CD measurements of BSA on QDs-COOH, to minimize contributions of unadsorbed BSA, excess QDs (20 nM) and a low concentration of BSA (5 nM) were used. After binding to QDs-COOH, a slight decrease of the helical structure was also observed (Figure 4b–d). This indicates only a small secondary structure change for BSA adsorbed on the QDs-COOH surface.

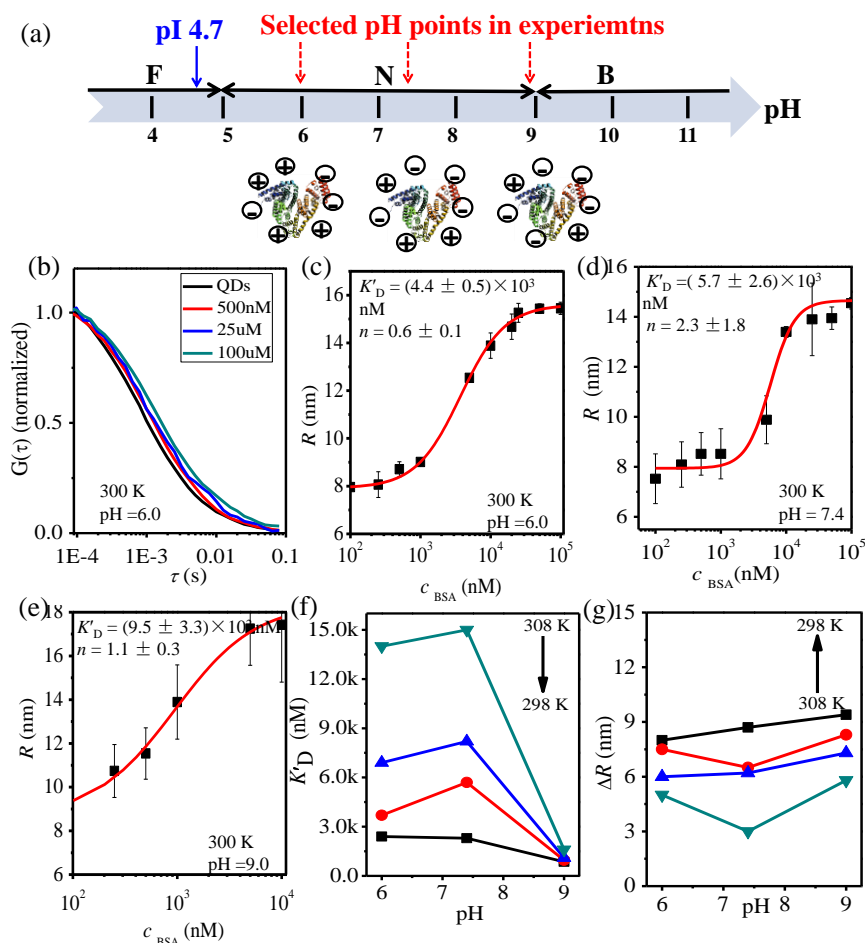


Figure 3. (a) Selected pH points for QDs-COOH and BSA binding in FCS measurements; (b) FCS correlation curves; (c–e) hydrodynamic radii of QDs-COOH at different pH (300 K); (f) K'_D at different temperatures and pH; and (g) the protein corona thickness at different temperatures and pH.

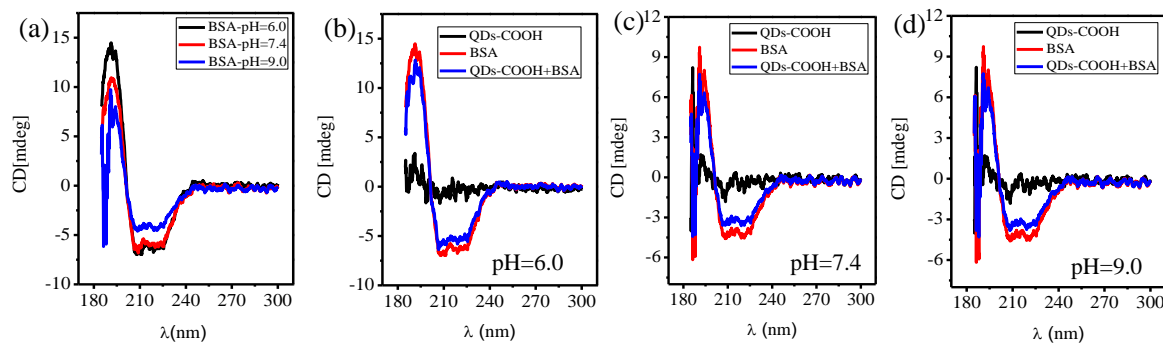


Figure 4. (a) Circular dichroism (CD) spectroscopy of bovine serum albumin (BSA) at different pH (6.0, 7.4, and 9.0); (b–d) CD of QDs-COOH, BSA, and a mixture of QDs-COOH (4 nM) and BSA (0.2 mM) at different pH (6.0, 7.4, and 9.0). In CD experiments, concentrations of QDs-COOH and BSA were 20 nM and 5 nM, respectively.

As a contrast, BSA adsorption on QDs-PEG at different pH in buffer solution was also investigated by FCS as a contrast (Figure S3). Due to the presence of PEG, no BSA adsorption was observed at room temperature, confirming that PEG can reduce the binding of proteins to nanoparticles [56].

3.4. Protein Binding in Whole Mice Serum and Plasma Samples

FCS measurements have also been used to measure the protein binding on QDs-COOH in serum and plasma samples of mice. Due to the absence of blood cells (especially red blood cells), no significant interference to FCS measurements was observed. The thickness of the protein corona (ΔR , corrected by the viscosity of serum and plasma) in plasma was found to be higher than that in serum and BSA solution (Figure 5). This may be due to more proteins and other chemicals with different sizes and affinities in plasma [57]. Additionally, the corona thickness is thinner at higher temperatures.

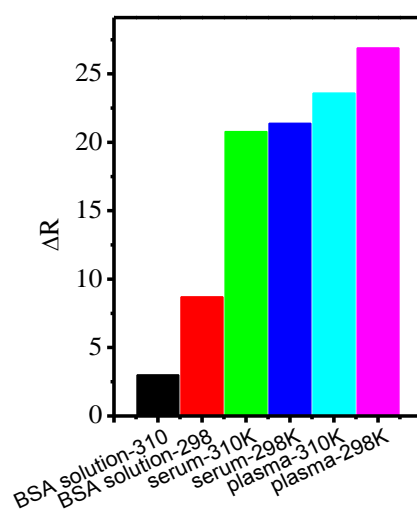
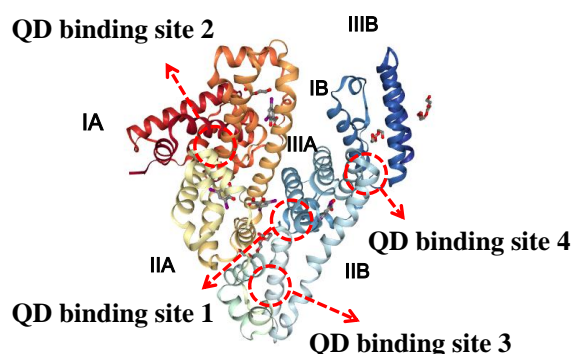


Figure 5. Protein corona thickness of quantum dots in plasma, serum, and BSA solution at different temperatures (298 and 310 K).

3.5. Simulation of BSA-QDs Interaction

Based on the structural analysis, four QD binding sites were identified in the BSA protein structure (as shown in Scheme 1). Binding site 1 resides in the central cavity of the BSA which is beneficial to the binding. Sites 2–4 are situated at the interface of two subdomains in the neighborhood (Site 2 resides at the interface between subdomains IA and IB. Site 3 resides at the interface between subdomains IIA and IIB, and site 4 resides at the interface between subdomains IIIA and IIIB) which contain substitutions of amino acids that create interactions across inter-domain boundaries within the BSA. There was a coordination of the carboxyl groups on the QDs with specific positively-charged amino acid residues which attributed to the high affinity by both electrostatic reaction and hydrogen-bonding interactions [42,43]. At pH 6.0, QDs were inclined to bind at binding sites 2–4 due to the electrostatic interactions formed by the residues with specific positive charges. At pH 7.4, QDs could bind to BSA in both the central cavity and the interface between neighborhood subdomains. However, at pH 9.0 QDs would prefer to bind with BSA in its central cavity (binding site 1) due to the favorable hydrogen bonding and hydrophobic interactions which lead to the higher binding capacity.



Scheme 1. The structure of BSA and the simulation result showing the location of the four binding sites (1–4) for QDs-COOH.

4. Conclusions

In summary, we have investigated the interaction between CdSe QDs and BSA to probe their temperature- and pH-dependent binding by FCS via measuring the microscopic dissociation constant K'_D , Hill coefficient n , and the thickness of the protein coronas in buffer solution, serum, and plasma. The binding of BSA to the QDs-COOH was found to be enthalpy-driven. The results also showed that the incensement of temperature was a disadvantage to the binding of protein and QDs, while pH had a profound and complex effect on the interaction by changing the structure of the BSA. This work also proved the effectiveness and accuracy of the FCS method to evaluate the kinetics and thermodynamic parameters of biomolecule interaction and the practicability of the FCS method in real serum and plasma samples. Finally, simulation results have showed four favored QD binding sites and different combination modes in BSA.

Supplementary Materials: The following are available online at <http://www.mdpi.com/2079-4991/7/5/93/s1>. Figure S1: FCS correlation curves and hydrodynamic radius of QDs-COOH at different BSA concentrations (pH = 6.0) and BSA concentrations, Figure S2: FCS correlation curves and hydrodynamic radius of QDs-COOH at different BSA concentrations (pH = 9.0) and BSA concentrations, Figure S3: (a) FCS correlation curves and (b–d) Hydrodynamic radius of QDs-PEG at different BSA concentrations (T = 298 K) at different pH.

Acknowledgments: This work was supported by the National Natural Science Foundation of China (21475071 and 21275082), the Taishan Scholar Program of Shandong (ts201511027), Strategic Priority Research Program of Chinese Academy of Sciences (XDA09040300), Beijing Science, Technology project (Z151100003915077), the Beijing Nova programme (Z15110000315081), and the Beijing Talents Fund (2015000021223ZK17).

Author Contributions: Qiyan Zhao, Zonghua Wang, and Liming Xie designed the project. Qiyan Zhao performed the experiments and analyzed the data; Menghua Cui assisted in data processing and the manuscript preparation; Ying Liu assisted in the mouse blood experiments; Shichao Pang and Jingfang Wang performed the computational simulation; and all authors contributed to the manuscript.

Conflicts of Interest: The authors declare no competing financial interest.

References

1. Maestro, L.M.; Ramirez-Hernandez, J.E.; Bogdan, N.; Capobianco, J.A.; Vetrone, F.; Sole, J.G.; Jaque, D. Deep tissue bio-imaging using two-photon excited CdTe fluorescent quantum dots working within the biological window. *Nanoscale* **2012**, *4*, 298–302. [[CrossRef](#)] [[PubMed](#)]
2. Qi, X.P.; Huang, Y.Y.; Lin, Z.S.; Xu, L.; Yu, H. Dual-Quantum-Dots-Labeled Lateral Flow Strip Rapidly Quantifies Procalcitonin and C-reactive Protein. *Nano Res. Lett.* **2016**, *11*, 167–175. [[CrossRef](#)] [[PubMed](#)]
3. Zhao, M.X.; Zhu, B.J. The Research and Applications of Quantum Dots as Nano-Carriers for Targeted Drug Delivery and Cancer Therapy. *Nano Res. Lett.* **2016**, *11*, 207–216. [[CrossRef](#)] [[PubMed](#)]
4. Lu, Z.S.; Li, C.M. Quantum Dot-Based Nanocomposites for Biomedical Applications. *Curr. Med. Chem.* **2011**, *18*, 3516–3528. [[CrossRef](#)] [[PubMed](#)]

5. Chen, J.; Li, C.; Zhao, D.W.; Lei, W.; Zhang, Y.; Cole, M.T.; Chu, D.P.; Wang, B.P.; Cui, Y.P.; Sun, X.W.; et al. A quantum dot sensitized solar cell based on vertically aligned carbon nanotube templated ZnO arrays. *Electrochem. Comm.* **2010**, *12*, 1432–1435. [[CrossRef](#)]
6. Vannoy, C.H.; Leblanc, R.M. Effects of DHLA-Capped CdSe/ZnS Quantum Dots on the Fibrillation of Human Serum Albumin. *J. Phys. Chem. B* **2010**, *114*, 10881–10888. [[CrossRef](#)] [[PubMed](#)]
7. Atay, Z.; Biver, T.; Corti, A.; Eltugral, N.; Lorenzini, E.; Masini, M.; Paolicchi, A.; Pucci, A.; Ruggeri, G.; Secco, F.; et al. Non-covalent interactions of cadmium sulphide and gold nanoparticles with DNA. *J. Nanopart. Res.* **2010**, *12*, 2241–2253. [[CrossRef](#)]
8. Li, J.H.; Zhang, Y.; Xiao, Q.; Tian, F.F.; Liu, X.R.; Li, R.; Zhao, G.Y.; Jiang, F.L.; Liu, Y. Mitochondria as target of quantum dots toxicity. *J. Hazard. Mater.* **2011**, *194*, 440–444. [[CrossRef](#)] [[PubMed](#)]
9. Lu, Z.S.; Li, C.M.; Bao, H.F.; Qiao, Y.; Toh, Y.H.; Yang, X. Mechanism of Antimicrobial Activity of CdTe Quantum Dots. *Langmuir* **2008**, *24*, 5445–5452. [[CrossRef](#)] [[PubMed](#)]
10. Guo, G.N.; Liu, W.; Liang, J.G.; He, Z.K.; Xu, H.B.; Yang, X.L. Probing the cytotoxicity of CdSe quantum dots with surface modification. *Mater. Lett.* **2007**, *61*, 1641–1644. [[CrossRef](#)]
11. Hoshino, A.; Fujioka, K.; Oku, T.; Suga, M.; Sasaki, Y.F.; Ohta, T.; Yasuhara, M.; Suzuki, K.; Yamamoto, K. Physicochemical properties and cellular toxicity of nanocrystal quantum dots depend on their surface modification. *Nano Lett.* **2004**, *4*, 2163–2169. [[CrossRef](#)]
12. Donaldson, K.; Brown, D.; Clouter, A.; Duffin, R.; MacNee, W.; Renwick, L.; Tran, L.; Stone, V. The pulmonary toxicology of ultrafine particles. *J. Aerosol Med.* **2002**, *15*, 213–220. [[CrossRef](#)] [[PubMed](#)]
13. Safi, M.; Courtois, J.; Seigneuret, M.; Conjeaud, H.; Berret, J.F. The effects of aggregation and protein corona on the cellular internalization of iron oxide nanoparticles. *Biomaterials* **2011**, *32*, 9353–9363. [[CrossRef](#)] [[PubMed](#)]
14. Xiao, J.B.; Chen, L.S.; Yang, F.; Liu, C.X.; Bai, X.L. Green, yellow and red emitting CdTe QDs decreased the affinities of apigenin and luteolin for human serum albumin in vitro. *J. Hazard Mater.* **2010**, *182*, 696–703. [[CrossRef](#)] [[PubMed](#)]
15. Idowu, M.; Lamprecht, E.; Nyokong, T. Interaction of water-soluble thiol capped CdTe quantum dots and bovine serum albumin. *J. Photochem. Photobiol. A* **2008**, *198*, 7–12. [[CrossRef](#)]
16. Sun, H.Y.; Yang, X.D.; Li, M.; Han, S.L.; Liu, Y.X.; Tan, X.J.; Liu, C.G.; Liu, R.T. Insights into the effect of N-acetyl-L-cysteine-capped CdTe quantum dots on the structure and activity of human serum albumin by spectroscopic techniques. *J. Lumin.* **2015**, *167*, 1–7. [[CrossRef](#)]
17. Xiao, J.B.; Bai, Y.L.; Wang, Y.F. Systematic investigation of the influence of CdTe QDs size on the toxic interaction with human serum albumin by fluorescence quenching method. *Spect. Acta Part A* **2010**, *76*, 93–97. [[CrossRef](#)] [[PubMed](#)]
18. Milohum, M.D.; Valentin, C.; Monica, I.; Messanh, A.M.; Simion, A. Study of the interaction between CdSe/ZnS core-shell quantum dots and bovine serum albumin by spectroscopic techniques. *J. Photochem. Photobiol. A Chem.* **2010**, *215*, 118–122.
19. He, Y.Q.; Yin, P.F.; Gong, H.P.; Peng, J.J.; Liu, S.P. Characterization of the interaction between mercaptoethylamine capped CdTe quantum dots with human serum albumin and its analytical application. *Sens. Actuators B* **2011**, *157*, 8–13. [[CrossRef](#)]
20. Cui, M.H.; Liu, R.X.; Deng, Z.Y.; Ge, G.L.; Liu, Y.; Xie, L.M. Quantitative study of protein coronas on gold nanoparticles with different surface modifications. *Nano Res.* **2014**, *7*, 345–352. [[CrossRef](#)]
21. Mamedova, N.N.; Kotov, N.A.; Rogach, A.L.; Studer, J. Albumin-CdTe nanoparticle bioconjugates: Preparation, structure, and interunit energy transfer with antenna effect. *Nano Lett.* **2001**, *1*, 281–286. [[CrossRef](#)]
22. Pinaud, F.; King, D.; Moore, H.-P.; Weiss, S. Bioactivation and cell targeting of semiconductor CdSe/ZnS nanocrystals with phytochelatin-related peptides. *J. Am. Chem. Soc.* **2004**, *126*, 6115–6123. [[CrossRef](#)] [[PubMed](#)]
23. Hess, S.T.; Huang, S.H.; Heikal, A.A.; Webb, W.W. Biological and chemical applications of fluorescence correlation spectroscopy: A review. *Biochemistry* **2002**, *41*, 697–705. [[CrossRef](#)] [[PubMed](#)]
24. Haustein, E.; Schwille, P. Ultrasensitive investigations of biological systems by fluorescence correlation spectroscopy. *Methods* **2003**, *29*, 153–166. [[CrossRef](#)]

25. Wohland, T.; Friedrich, K.; Hovius, R.; Vogel, H. Study of ligand–receptor interactions by fluorescence correlation spectroscopy with different fluorophores: Evidence that the homopentameric 5-hydroxytryptamine type 3a_s receptor binds only one ligand. *Biochemistry* **1999**, *38*, 8671–8681. [[CrossRef](#)] [[PubMed](#)]
26. Schubert, F.; Zettl, H.; Hafner, W.; Krauss, G.; Krausch, G. Comparative thermodynamic analysis of DNA–protein interactions using surface Plasmon resonance and fluorescence correlation spectroscopy. *Biochemistry* **2003**, *42*, 10288–10294. [[CrossRef](#)] [[PubMed](#)]
27. Ling, C.H.; Gosch, M.; Lasser, T.; Wohland, T. Simultaneous multicolor fluorescence cross-correlation spectroscopy to detect higher order molecular interactions using single wavelength laser excitation. *Biophys. J.* **2006**, *91*, 715–727.
28. Pack, C.G.; Aoki, K.; Taguchi, H.; Yoshida, M.; Kinjo, M.; Tamura, M. Effect of electrostatic interactions on the binding of charged substrate to GroEL studied by highly sensitive fluorescence correlation spectroscopy. *Biochem. Biophys. Res. Commun.* **2000**, *267*, 300–304. [[CrossRef](#)] [[PubMed](#)]
29. Wang, Y.; Tang, Z.; Kotov, N.A. Bioapplication of nanosemiconductors. *Mater. Today* **2005**, *8*, 20–31. [[CrossRef](#)]
30. Clapp, A.R.; Medintz, I.L.; Mattoussi, H. Forster resonance energy transfer investigations using quantum-dot fluorophores. *Chem. Phys. Chem.* **2006**, *7*, 47–57. [[CrossRef](#)] [[PubMed](#)]
31. Ballou, B.; Lagerholm, B.C.; Ernst, L.A.; Bruchez, M.P.; Waggoner, A.S. Noninvasive imaging of quantum dots in mice. *Bioconj. Chem.* **2004**, *15*, 79–86. [[CrossRef](#)] [[PubMed](#)]
32. Sun, B.; Xie, W.; Yi, G.; Chen, D.; Zhou, Y.; Cheng, J. Microminiaturized immunoassays using quantum dots as fluorescent label by laser confocal scanning fluorescence detection. *J. Immunol. Methods* **2001**, *249*, 85–89. [[CrossRef](#)]
33. Li, L.; Qian, H.F.; Fang, N.H.; Ren, J.C. Significant enhancement of the quantum yield of CdTe nanocrystals synthesized in aqueous phase by controlling the pH and concentrations of precursor solutions. *J. Lumin.* **2006**, *116*, 59–66. [[CrossRef](#)]
34. Christensen, S.D.; Mikkelsen, L.F.; Fels, J.J.; Bodvarsdottir, T.B.; Hansen, A.K. Quality of plasma sampled by different methods for multiple blood sampling in mice. *Lab Anim.* **2009**, *43*, 65–71. [[CrossRef](#)] [[PubMed](#)]
35. Dong, M.D.; Martinez, M.M.; Mayer, M.F.; Pappas, D. Single molecule fluorescence correlation spectroscopy of single apoptotic cells using a red-fluorescent caspase probe. *Analyst* **2012**, *137*, 2997. [[CrossRef](#)] [[PubMed](#)]
36. Röcker, C.; Pötzl, M.; Zhang, F.; Parak, W.J.; Nienhaus, G.U. A quantitative fluorescence study of protein monolayer formation on colloidal nanoparticles. *Nat. Nanotechnol.* **2009**, *4*, 577–580. [[CrossRef](#)] [[PubMed](#)]
37. Tsai, D.H.; DelRio, F.W.; Keene, A.M.; Tyner, K.M.; MacCuspie, R.I.; Cho, T.J.; Zachariah, M.R.; Hackley, V.A. Adsorption and conformation of serum albumin protein on gold nanoparticles investigated using dimensional measurements and in situ spectroscopic methods. *Langmuir* **2011**, *27*, 2464–2477. [[CrossRef](#)] [[PubMed](#)]
38. Lacerda, S.H.D.P.; Park, J.J.; Meuse, C.; Pristiniski, D.; Becker, M.L.; Karim, A.; Douglas, J.F. Interaction of gold nanoparticles with common human blood proteins. *ACS Nano* **2010**, *4*, 365–379. [[CrossRef](#)] [[PubMed](#)]
39. Bujacz, A. Structure of bovine, equine and leporine serum albumin. *Acta Crystallogr. D Biol. Crystallogr.* **2012**, *68*, 1278–1289. [[CrossRef](#)] [[PubMed](#)]
40. Huang, J.; Rauscher, S.; Nawrocki, G.; Ran, T.; Feig, M.; de Groot, B.L.; Grubmuller, H.; MacKerell, A.D., Jr. CHARMM36m: An improved force field for folded and intrinsically disordered proteins. *Nat. Methods* **2016**, *14*, 71–73. [[CrossRef](#)] [[PubMed](#)]
41. Philips, J.C.; Braun, R.; Wang, W.; Gumbart, J.; Tajkhorshid, E.; Villa, E.; Chipot, C.; Skeel, R.D.; Kale, L.; Schulten, K. Scalable molecular dynamics with NAMD. *J. Comput. Chem.* **2005**, *26*, 1781–1802. [[CrossRef](#)] [[PubMed](#)]
42. Xiao, Q.; Huang, S.; Qi, Z.D.; Zhou, B.; He, Z.K.; Liu, Y. Conformation, thermodynamics and stoichiometry of HSA adsorbed to colloidal CdSe/ZnS quantum dots. *BBA Proteins Proteom.* **2008**, *1784*, 1020–1027. [[CrossRef](#)] [[PubMed](#)]
43. Cistola, D.P.; Small, D.M.; Hamilton, J.A. Carbon 13 NMR studies of saturated fatty acids bound to bovine serum albumin: II. Electrostatic interactions in individual fatty acid binding sites. *J. Biol. Chem.* **1987**, *262*, 10980–10985. [[PubMed](#)]
44. Hamilton, J.A.; Era, S.; Bhamidipati, S.P.; Reed, R.G. Locations of the three primary binding sites for long-chain fatty acids on bovine serum albumin. *Proc. Natl. Acad. Sci. USA* **1991**, *88*, 2051–2054. [[CrossRef](#)] [[PubMed](#)]

45. Parks, J.S.; Cistola, D.P.; Small, D.M.; Hamilton, J.A. Interactions of the carboxyl group of oleic acid with bovine serum albumin: A ¹³C-NMR study. *J. Biol. Chem.* **1983**, *258*, 9262–9269. [[PubMed](#)]
46. Subhajt, G.; Joykrishna, D. Interaction of bovine serum albumin with N-acyl amino acid based anionic surfactants: Effect of head-group hydrophobicity. *J. Colloid Int. Sci.* **2015**, *458*, 284–292.
47. Li, D.J.; Zhang, T.; Xu, C.; Ji, B.M. Effect of pH on the interaction of vitamin B12 with bovine serum albumin by spectroscopic approaches. *Spectrochim. Acta Part A* **2011**, *83*, 598–608. [[CrossRef](#)] [[PubMed](#)]
48. Dockal, M.; Carter, D.C.; Ruker, F. Conformational Transitions of the Three Recombinant Domains of Human Serum Albumin Depending on pH. *J. Biol. Chem.* **2000**, *275*, 3042–3050. [[CrossRef](#)] [[PubMed](#)]
49. Salis, A.; Bostrom, M.; Medda, L.; Cugia, F.; Barse, B.; Parsons, D.F.; Ninham, B.W.; Monduzzi, M. Measurements and Theoretical Interpretation of Points of Zero Charge/Potential of BSA Protein. *Langmuir* **2011**, *27*, 11597–11604. [[CrossRef](#)] [[PubMed](#)]
50. Chan, V.W.F.; Jorgensen, A.M.; Borders, C.L. Inactivation of bovine thrombin by water-soluble carbodiimides: The essential carboxyl group has a pKa of 5.51. *Biochem. Biophys. Res. Commun.* **1988**, *151*, 709–716. [[CrossRef](#)]
51. Ding, Y.H.; Shu, Y.; Ge, L.L.; Guo, R. The effect of sodium dodecyl sulfate on the conformation of bovine serum albumin. *Colloids Surf. A* **2007**, *298*, 163–169. [[CrossRef](#)]
52. Sen, P.; Ahmad, B.; Khan, R.H. Formation of a molten globule like state in bovine serum albumin at alkaline pH. *Eur. Biophys. J.* **2008**, *37*, 1303–1308. [[CrossRef](#)] [[PubMed](#)]
53. Caetano, W.; Amaral, C.L.C.; Itri, R. The influence of urea on the structure of proteins in reversed micelles. *Int. J. Biol. Macromol.* **2013**, *53*, 42–53. [[CrossRef](#)]
54. Qu, P.; Wang, Y.X.; Wu, G.H. Effect of polyethylene glycols on the alkaline-induced molten globule intermediate of bovine serum albumin. *Int. J. Biol. Macromol.* **2012**, *51*, 97–104. [[CrossRef](#)] [[PubMed](#)]
55. Chatterjee, S.; Srivastava, T.S. Spectral investigations of the interaction of some porphyrins with bovine serum albumin. *J. Porphyr. Phthalocyanines* **2000**, *4*, 147–157. [[CrossRef](#)]
56. Walkey, C.D.; Olsen, J.B.; Guo, H.B.; Emili, A.; Chan, W.C.W. Nanoparticle size and surface chemistry determine serum protein adsorption and macrophage uptake. *J. Am. Chem. Soc.* **2012**, *134*, 2139–2147. [[CrossRef](#)] [[PubMed](#)]
57. Mirshafiee, V.; Kim, R.; Mahmoudi, M.; Kraft, M.L. The importance of selecting a proper biological milieu for protein corona analysis in vitro: Human plasma versus human serum. *Int. J. Biochem. Cell Biol.* **2016**, *75*, 188–195. [[CrossRef](#)] [[PubMed](#)]



© 2017 by the authors. Licensee MDPI, Basel, Switzerland. This article is an open access article distributed under the terms and conditions of the Creative Commons Attribution (CC BY) license (<http://creativecommons.org/licenses/by/4.0/>).